Experimental and CFD investigations on full volumetric flow to a solar flat-plate glass collector

Pascal Leibbrandt, Thomas Schabbach, Michael Dölz, Martin Rhein

Institut für Regenerative Energietechnik, University of Applied Sciences Nordhausen (Germany)

Summary

In the project solar flat-plate glass collector, a new type of solar collector will be developed which, simplified, consists of 4 glass plates. As subgoal of the project the full volumetric flow and heat transfer in the fluid layer and the collector filling have been examined experimentally and numerically. The experimental setup and the CFD settings are presented. By comparison of experimental data and CFD results the simulation results were checked. It appeared that the CFD simulations are able to model the flow well, so an optimization of the flow and heat transfer in the layer can be carried out numerically.

Keywords: glass collector, fluid distribution, CFD, validation, filling process

1. Collector construction and function

In context of the research project "Nurglassolarflachkollektor" a collector with lower production costs will be developed, which consists primarily of glass. Due to the simplified construction cost intensive production steps such as the absorber welding will be unnecessary and enable an automated production process with fewer production steps. Manufacturing costs can thus be reduced by approximately 20% compared to conventional standard flat-plate collectors. Another advantage is the reduced collector height of <50 mm, which allows a simplified installation and collector field connection, so that other application areas (especially in facade) can be opened up.

The glass collector consists of four planar glass plates, which are glued and sealed by a frame and a fluid layer structure. As shown in Fig. 1 the heat transfer medium passes directly through the middle rectangular disk-space. The coatings on the glasses ensure optimal radiation absorption in the fluid layer and minimize the radiation losses due to reflection and emission, see also Leibbrandt et al. (2014). Insulating gas layers minimize convective heat losses to the front and back. As also shown in Fig.1, the heat transfer fluid has to be distributed full volumetric from the circular collector connection through the flow channel. Without adequate installations in the fluid layer a short-circuit flow would be the follow. The fluid layer structure should also be able to absorb inner/outer forces from/to the fluid layer.
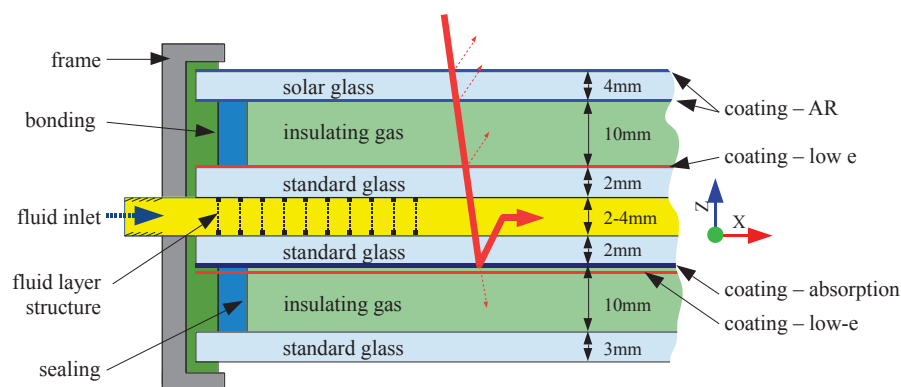

Fig. 1: Construction of the glass collector

Beside the presented problem of the fluid layer flow also the flow in the insulating gas layer, see Leibbrandt et al. (2016) and structural mechanical questions about the glass loads (Rhein et al. (2016)) are investigated in the project. With a specially developed collector test rig collector prototypes are investigated parallel to the project (see Dölz et al. (2016)).

2. Full volumetric flow and heat transfer

The flow in the fluid layer should be optimized so that the absorbed radiation energy is transported ideally from the absorption layer to the heat carrier fluid. The collector efficiency factor is:

$$F' = \frac{U_{int}}{U_{int} + U_{loss}}$$

(eq. 1)

U_{int} is the internal heat transfer coefficient, which describes just the forced convection in the fluid layer here, U_{loss} describes the overall heat transfer losses of the whole collector. So, F' is the theoretical ratio of the useful energy gain to the useful gain that would result if the absorbing surface would be at the fluid temperature, Duffie Beckman (2013). The collector efficiency factor is at its maximum if the flow would be full volumetric. For flat-plate collectors with a fin width of 90-120 mm, the collector efficiency factor is about 88-94%, Wesselak et al. (2013). The heat transfer is at its maximum when the flow is fully homogeneous (without flow areas with no/low flow velocity) and turbulent.

At the same time the pressure drop and the filling/drainback performance must be ensured for a potentially drainback system application.

The rectangular flow channel has a length L, a width B and a thickness of s_F (see Fig. 2). For the analysis presented here the collector size is LxB = 2000x1000 mm, the fluid layer thickness s_F varies between 2 and 10 mm. The fluid layer is inclined at an angle φ against the horizontal.
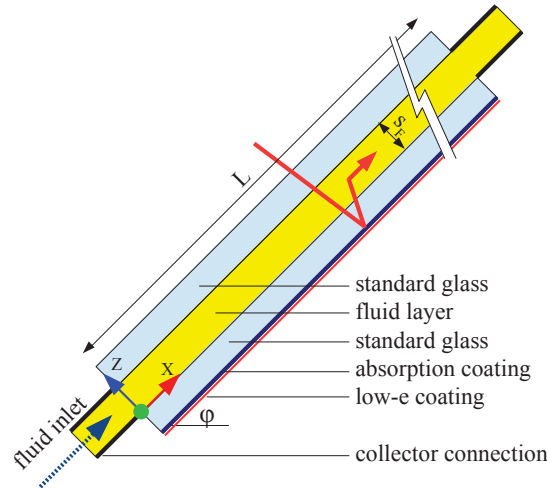

Fig. 2: Problem definition

Starting from a circular collector connection the heat transfer fluid should be distributed ideally. The flow velocity $\vec{u_i}$ at any point i of the fluid layer field consists of the flow velocity components u_i, v_i and w_i - see Fig. 3(a).

$$\vec{u_i} = \begin{pmatrix} u_i(x,y,z) \\ v_i(x,y,z) \\ w_i(x,y,z) \end{pmatrix}$$

(eq. 2)

In case of homogeneous flow, the flow velocity $\overrightarrow{u_{i,opt}}$ is the same at all points of the fluid layer and consists only of velocity components in the main flow direction - see Fig. 3(b).

$$\overrightarrow{u_{i,opt}} = \begin{pmatrix} u_i(x) \\ 0 \\ 0 \end{pmatrix}$$

(eq. 3)
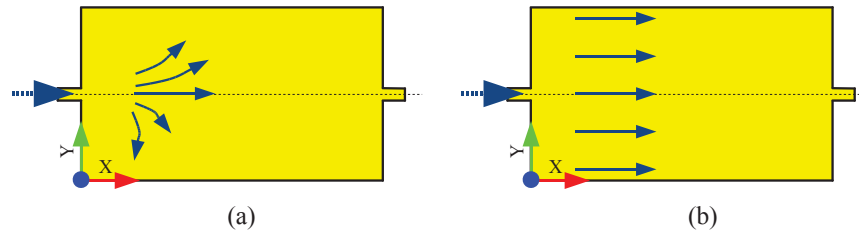
Fig. 3: Flow types in the fluid layer

For the experimental investigation of the flow behavior in the fluid layer 2 glasses in size of 2000x1000x4 mm each were glued and sealed with a 10 mm aluminum spacer in between. Later, the fluid film thickness will be reduced to up to 2-4 mm. For stabilization of the fluid layer the glasses were fixed with mounting rails in the experimental setup – see Fig. 4.

For volume flow generation and pressure control a laboratory thermostat was used, so that the fluid temperature could be adjusted and kept constant. Volume flow rate, in-/outlet temperatures and the pressure drop were determined.

The fluid was enriched with particles before the collector inlet via an injector pipe to visualize the flow behavior. The particle selection was based on a number of preliminary tests. Based on practicality, slip behavior and density expanded glass granulate, ceramic microspheres, polyester plates and soda-lime glass balls were tested. The particles had to be able to reflect the incoming light well. They should be small enough to have no effect on the flow and ensure a slip-free behavior in contrast to the fluid. Also different lighting media, such as halogen spotlights, fluorescent lighting tubes and led were tested.
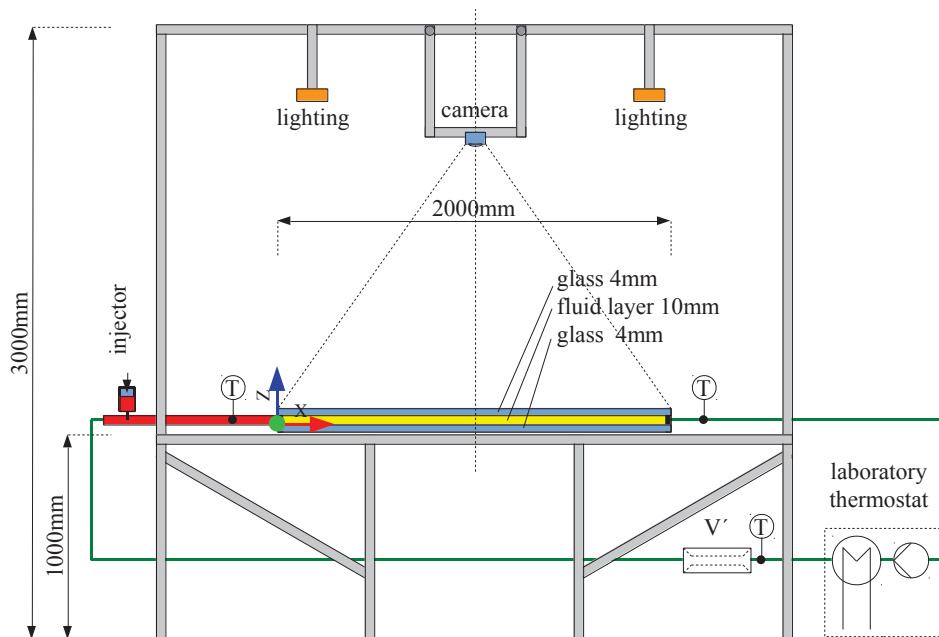
Fig. 4: Test setup full volumetric flow

The flow field was recorded with an HD-camera (50 frames/sec) from above. The generated single images were aligned, optimized and transferred to an image stack by using an image processing program. That image stack was transformed to a single image by subtraction, so it was possible to visualize the trail of the particles and to identify areas with low velocity. Ideally, the flow velocity should be identical in all points in the layer (see above).

So, three versions of different fluid layer structures (V00 - V02, see Fig. 5) were initially investigated experimentally. The inlet and outlet was located centrally on the short side of the fluid layer.

- In version V00 the fluid flows through the fluid layer without any internals.
- In version V01 the fluid is slowed right after the inlet with a central small barrier (width = 100 mm) and is so distributed sideways.
- Version V02 features a wide barrier (width = 900 mm) which directs the fluid to the long fluid layer wall.

Moreover, the experimental investigated versions V00 - V02 were simulated numerically using a simplified 2D CFD model. By preliminary investigations, the numerical discretization, the choice of flow and turbulence models and the admissibility of the 2D simplification ($z = 0$) were tested and validated. The boundary conditions were in all experimental analysis and simulations set identical to

$$\dot{V} = 140 \frac{l}{h} \qquad p \approx 1 \, bar \qquad T \approx 20°C.$$

As shown in Fig. 5, there is a good correlation between experimental and numerical data. In version V00 qualitatively similar flow swirls are identifiable. In versions V01 and V02 the distribution of the fluid to the edges agrees qualitatively in experiment and CFD results. Therefore, it can be assumed for additional versions that the CFD model provides sufficiently results and can be used to optimize the fluid distribution better than in the reference experiment V00. In addition, the option will be tested, to measure the velocity field locally with Prandtl tubes for example.
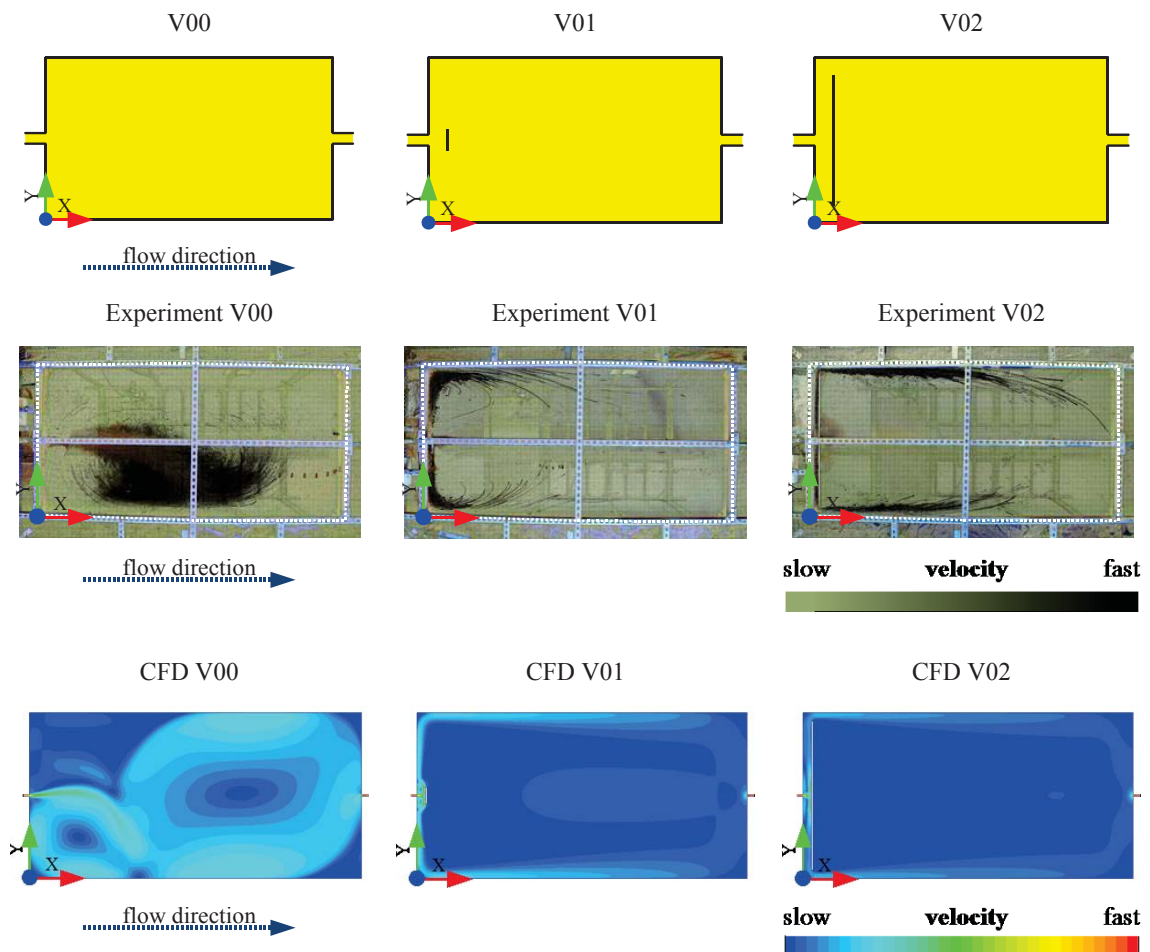

Fig. 5: Comparison of velocity distribution (middle: experiment, bottom: CFD)

After the qualitative validation of the CFD simulations additional fluid layer structures (V03-V08) were investigated numerically. So the optimization could be done more quickly. The experimental investigations took about 2-3 days per version, the simulation time was about a few hours per version.

The analysis of the homogeneity was carried out with the qualitative evaluation of flow visualization and the standard deviation of flow velocities u_i from the CFD simulations. It is:
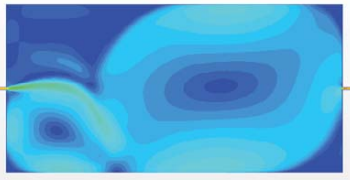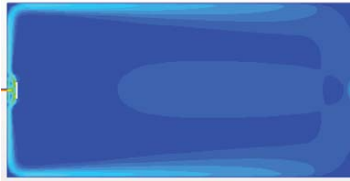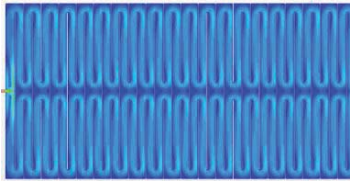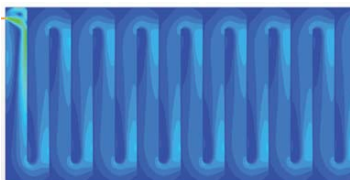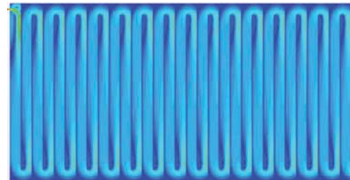
$$std = \sqrt{\frac{1}{n}\sum_{i=1}^{n}\left(u_i - \frac{1}{n}\sum_{i=1}^{n}u_i\right)^2} \qquad \text{(eq. 4)}$$

Also the pressure loss was read from the simulation data. In these 2D simulations, the pressure loss is determined over a reference layer thickness without any boundary layer influence. It is:

$$\Delta p = p_{inlet} - p_{outlet} \qquad \text{(eq. 5)}$$

For better overview these criteria are represented relative to the reference version V00.

Tab. 1: Velocity distribution, standard deviation and pressure loss V00 – V08

V00	V01	V02
std = 100% Δp = 100%	std = 100,2% Δp = 102.3%	std = 95.4% Δp = 101.6%
V03	**V04**	**V05**
std = 99.2% Δp = 104.1%	std = 82.5% Δp = 124.3%	std = 92.5% Δp = 101.0%
V06	**V07**	**V08**
std = 98.2% Δp = 105.0%	std = 88.1% Δp = 106.7%	std = 77.6% Δp = 159.6%

Results:

- V00, V03: In fluid channels with central inflow on the short collector side without fluid layer structures occur a flow expansion and thus a lowering of the average flow velocity. Generally, two flow swirls arise. The main flow direction tends thereby to a collector side, the other is barely flowed. For s_F = 2 mm and ideal distribution is Re = 78.

- V01, V02 and V05: In fluid channels with central inflow on the short collector side with fluid layer structures at the collector inlet a flow distribution to the long collector sides occurs. The fluid layer structures at the inlet are not able to distribute to the fluid over the whole collector length.

- V04, V06 – V08: In fluid channels with inflow on the short collector side with fluid layer structures the fluid is distributed optimally. From reasons of material saving, manufacturability and an ease of installation, fluid layer structures with lateral inlets (V06-V08) are appropriate preferable. The choice of the resultant channel width and geometry influence can be made regarding to flow homogeneity and thus to heat transfer. For s_F = 2 mm and good distribution (V08) is Re = 1213.

Also other structures have been tested so far, which are capable to distribute the heat transfer fluid quite well. As expected the pressure loss rises for more complex fluid layer structures. Especially in the versions V04, V06-V08 the fluid layer structure is able to connect the fluid layer glasses. The result is a sandwich structure which is able to carry internal and external loads from/to the fluid channel.

The CFD optimized fluid layer structures will be investigated experimentally in the further proceeding of the project. In addition, there are first collector prototypes under construction, which also will be tested on the collector test rig. This prototype studies will be supported by additional 3D CFD and FEM investigations with regard to the fluid distribution and the glass loads analysis.

After the optimization of the fluid layer structure, the influence on heat transfer was investigated. For this purpose, a 3D CFD model with the boundary conditions, as shown in Fig. 6, was used. The fluid layers' dimension was set to LxBxs$_F$ = 2000x1000x10 mm. The inclination of the layer was 45°. For these simulations 3 fluid layer structures, similar to versions V00, V06 and V07 were analyzed. The backside of the fluid channel has been set up with a constant heat flow density $\dot{q}_{abs}$ which corresponds to the absorbed solar radiation power. At the front convective heat transfer with a constant heat transfer coefficient and fixed ambient temperature was assumed. In reality the convective heat transfer coefficient depends on the front side temperature. The edges of the fluid channel have been supposed to be adiabatic. The fluid inlet temperature was set to 20°C; the inlet velocity was varied between 0.25 – 1.00 m/s (35 – 140 l/(m² h)).
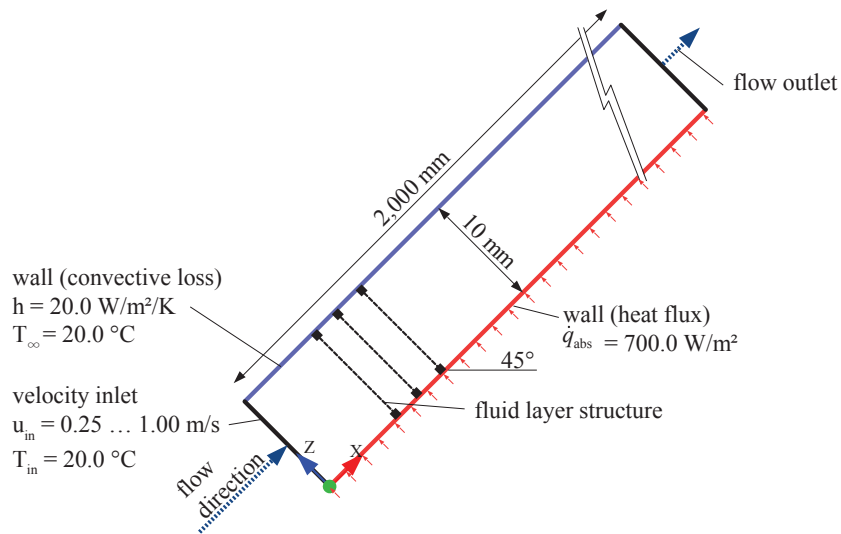

Fig. 6: CFD setup heat transfer

To rate the quality of the heat transfer through the fluid layer the useable enthalpy-flow $\dot{q}_{use}$ at the layer outlet was set into relation to mean fluid temperature difference. It is:

$$h_f = \frac{\dot{q}_{use}}{\overline{T_{abs}} - \overline{T_f}}$$
(eq. 6)

To compare the collector efficiency factor of the fluid layer F_f' with standard flat-plate collectors it is assumed, that the overall loss heat transfer coefficient $U_{loss} = 4\,W/(m^2 K)$. U_{loss} describes the collector heat losses over the sides and the back of the collector which are not part of the presented CFD simulations. The efficiency factor of the fluid layer F_f' is:

$$F_f' = \frac{h_f}{h_f + U_{loss}} \qquad\qquad \text{(eq. 7)}$$

Tab. 2: Influence of fluid layer structures on heat transfer (3D CFD results)

		u_{in} in m/s		
		0.25	0.50	1.00
fluid layer structure V00	$\dot{q}_{use}$ in W/m²	565.95	630.53	657.35
	h_f in W/m²/K	372.86	365.07	360.68
	F_f'	**98.9%**	**98.9%**	**98.9%**
fluid layer structure V06	$\dot{q}_{use}$ in W/m²	558.99	628.45	658.76
	h_f in W/m²/K	337.87	327.60	405.85
	F_f'	**98.8%**	**98.8%**	**99.0%**
fluid layer structure V07	$\dot{q}_{use}$ in W/m²	556.11	617.33	651.18
	h_f in W/m²/K	343.25	421.14	625.53
	F_f'	**98.8%**	**99.1%**	**99.4%**

The temperature distribution is shown in Fig. 7. In the versions V06 and V07 a temperature inhomogeneity can be seen especially at the end of the individual fluid channels. They are formed due to the lower flow velocity and lead to local temperature maxima (hot spots). They should be minimized by a suitable flow guidance. At these hotspots the heat transfer reduces and high temperature gradients occur which also lead to stresses in the glasses.
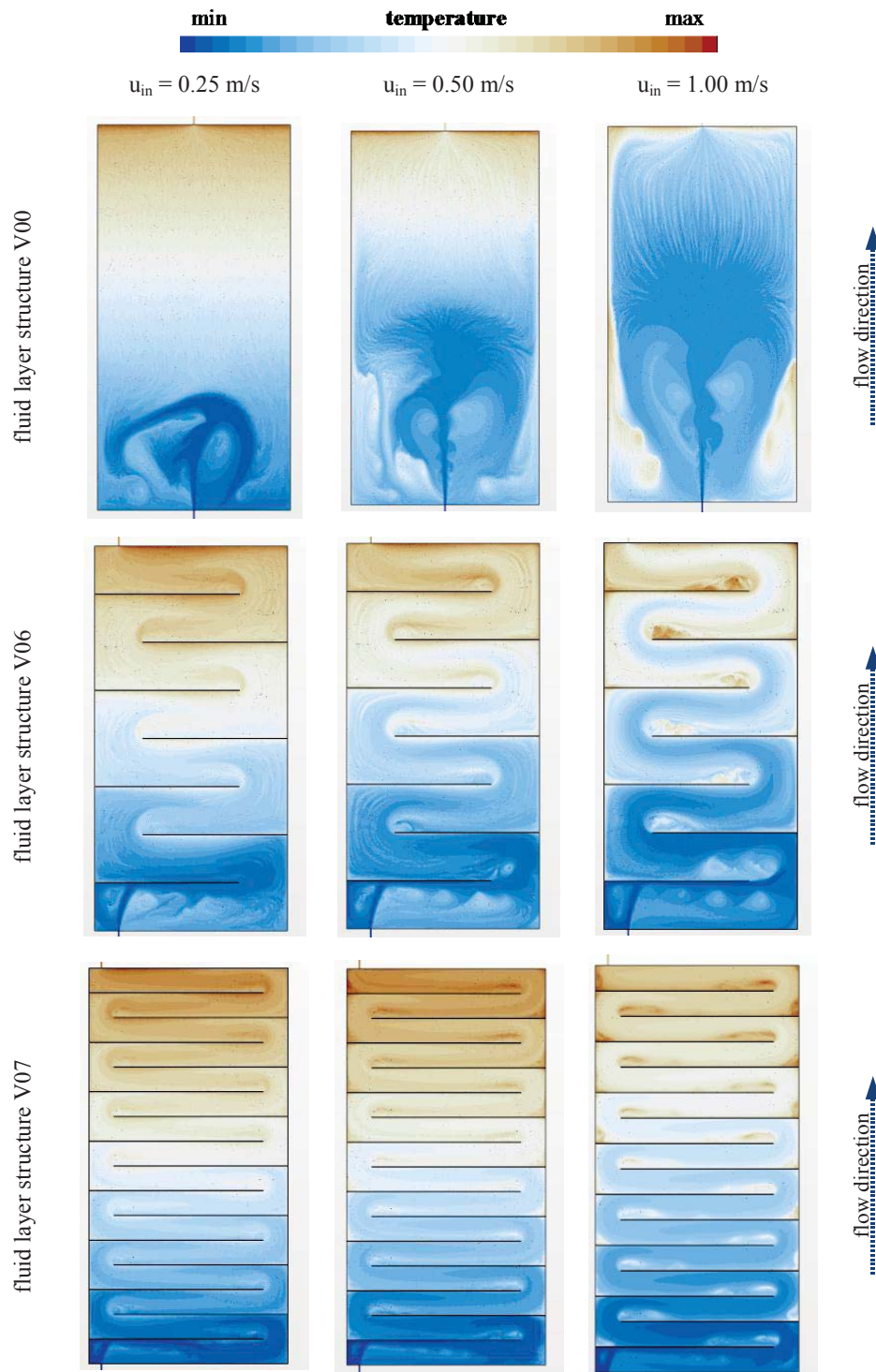
Fig. 7: Influence of fluid layer structures on temperature distribution (3D CFD results)

The versions with fluid channels as fluid layer structures lead to the best results for fluid distribution and heat transfer. This was shown by using experimental investigations and CFD simulations of the fluid layer.

These results are used as input quantities for experiments and FEM simulations to optimize structural behavior of the collector and are used as guidelines for first collector prototype design.

3. Collector filling

As mentioned above, the collector should also be suitable for a potential drain back use. The fluid layer structure should not only ensure a homogeneous flow and a good heat transfer but should also allow a fast and gas-free filling and completely emptying of the collector.

For first assessment the filling behavior was tested on a smaller version of the fluid layer with the measurement of $LxBxs_F = 500x250x10$ mm. The fluid layer was confined with 4 mm single pane safety glass in the experiment. Target was an air-free filling in the least possible time. For this a simplified drainback system with open drainback reservoir, as shown in Fig. 8, was realized. A HD-camera gave the opportunity to have a detailed look to the fluid layer, detect gas bubbles and ascertain the filling time.
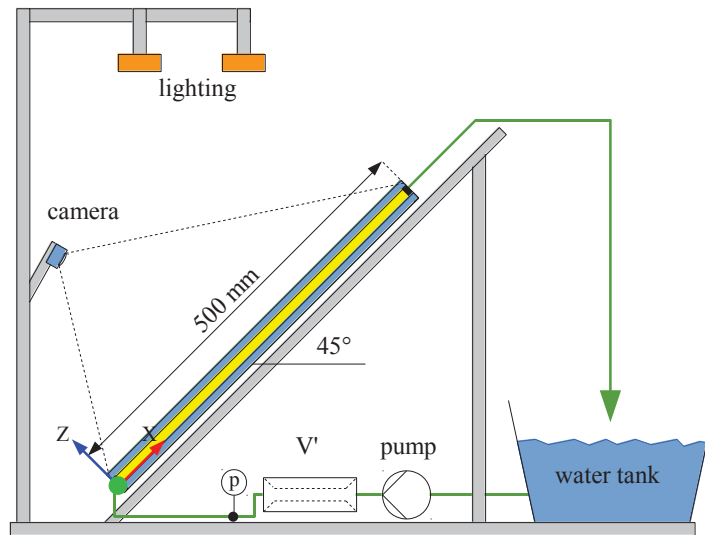

Fig. 8: Test setup collector filling

The lighting and contrast enhancement for better visualization of the bubbles were done with led spotlights and an all-around led belt on the glasses. The volume flow was generated with a pump after the drainback reservoir and was identified with an impeller counter.

The filling process is shown for different inlet velocities by single pictures in the interval of 10 seconds in Fig. 10.

- With the inlet velocity of $u_{in} = 2$ m/s the filling time was under 10 seconds. In addition to that, it is demonstrated, that a big amount of air bubbles is captured in the fluid layer. These air inclusions remain for several minutes in the collector. By internal flow rolls the air bubbles are circulated periodic in the fluid layer. Only by a short stop of the pump, the air bubbles can partially escape.

- With an inlet velocity of $u_{in} = 1$ m/s the filling time increased up to 12 seconds. The entry and circulation of air bubbles were reduced compared to the higher filling velocity. After 30 seconds of filling time there were just little bubbles at top of the fluid layer.

- Regarding to the proportionality the filling time increased up to 24 seconds with an inlet velocity of $u_{in} = 0.4$ m/s and after 30 seconds there are just a minimal amount of air inclusions left in the fluid layer. Compared to the higher filling velocities there was a worse venting of the upper corners to observe.
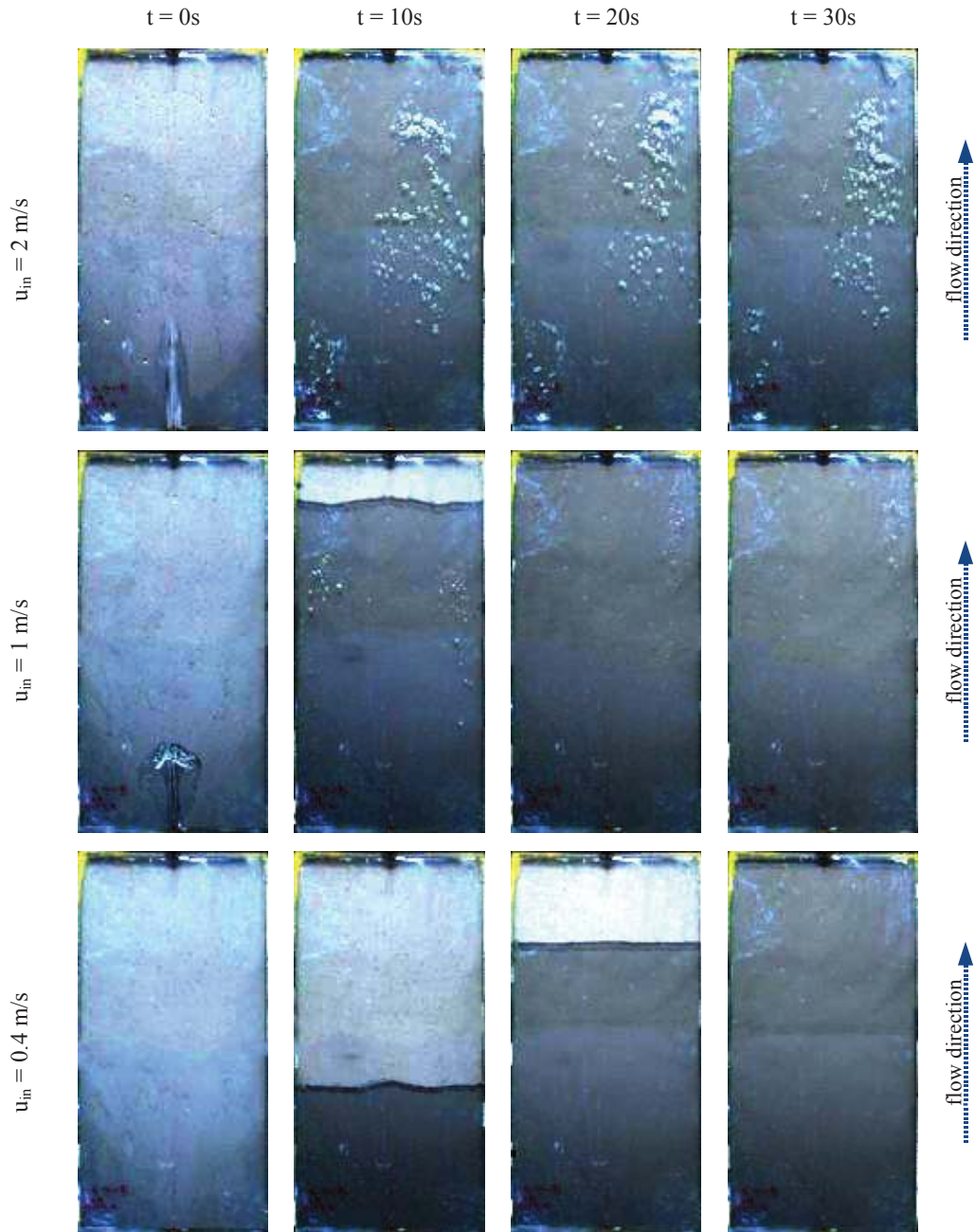
Fig. 9: Experimental results filling tests

In addition to these experimental investigations also CFD simulations on the filling behavior were carried out. In the simulations the fluid layer thickness was varied to check these influence on the filling behavior, too. For this purpose, a 3D CFD model inclined at an angle of 45° was used. Also a two-phase model which considered the interaction of the water and the air in the filling process was used. For better comparison of filling processes at different fluid layer thicknesses the fill level l_F was defined. This is the relationship of water volume in the fluid layer to the entire fluid layer volume.

$$l_F(t) = \frac{V_{water}\,(t)}{V_{total}} \qquad\qquad (\text{eq. 8})$$

Tab. 3 and Fig. 10 illustrate the results of the filling process with different fluid layer thicknesses and variable inlet velocities. For this simulations the inlet velocities were decreased in contrast to the experiments.

Tab. 3: Influence of filling velocity and fluid layer thickness on filling level l_F (3D CFD results)

		u_{in} in m/s		
		0.25	0.50	1.00
l_F (t=140s) in %	s_F = 10 mm	99.3	98.5	87.6
	s_F = 4 mm	99.8	96.9	78.1
	s_F = 2 mm	99.1	89.5	53.3

- For s_F = 10 mm there are good filling results for the both low filling velocities. Of course the filling process takes longer for the lowest velocity. Even for this fluid layer thickness a vent at the highest filling rate is only partially possible because of the forming of circulating air bubbles – see also experimental results.

- The behavior and the trend of poor ventability is proofed for smaller fluid layer thicknesses. For s_F = 4 mm an air free filling is even not possible for medium filling velocity. An air free filling for s_F = 2 mm is only possible with quite slow filling velocity.
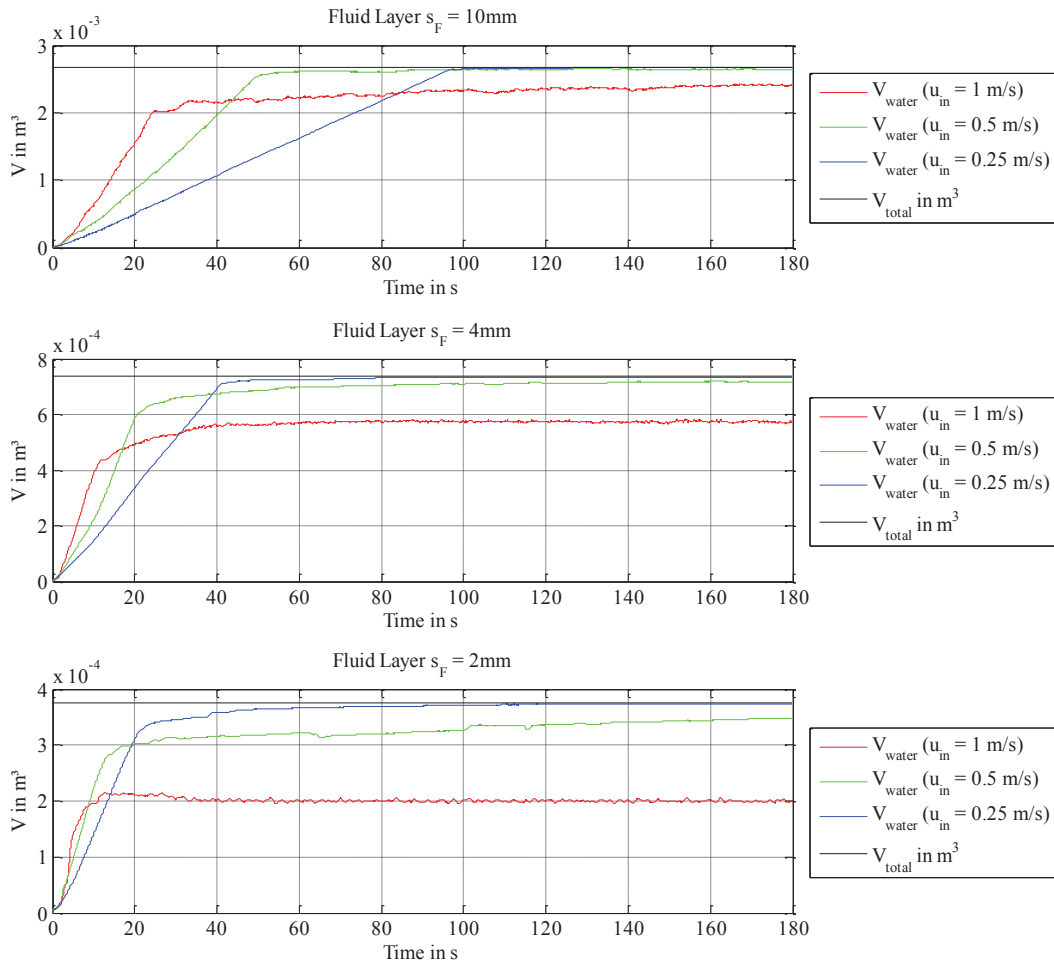

Fig. 10: Influence of filling velocity and fluid layer thickness on filling level (3D CFD results)

For the filling process therefore the lowest possible filling velocity should be chosen. In collectors and whole systems, the overall filling time will be the limiting factor. Further studies are needed to validate the filling behavior of collectors in the original scale with integrated fluid layer structure in addition to the presented results. Moreover, there will be a different filling behavior with water glycol mixture because of the varying material data.

4. Outlook

In continuation to the project additional fluid layer structures will be investigated experimentally and numerically. Target will be to increase the flow homogeneity, heat transfer and stability of the fluid layer. The pressure loss, manufacturability and long term stability must also be considered. The performance of the entire collector will be checked during QDT-testing in dependence of the different fluid layer structures. Mechanical load tests with internal and external forces will also take place.

5. Acknowledgement

6. References

Dölz; Schabbach; Leibbrandt; Rhein, 2016. Low-Cost-Kollektorprüfstand für quasidynamische Messungen im Hochtemperaturbereich. 26. OTTI Symposium Thermische Solarenergie, Bad Staffelstein

Duffie, Beckman, 2013. Solar Engineering of Thermal Processes, fourth ed. John Wiley & Sons Inc., Hoboken, New Jersey

Leibbrandt; Schabbach; Dölz; Rhein, 2016. CFD-Untersuchungen zu konvektiven Wärmeverlusten in Scheibenzwischenräumen mit großem Seitenverhältnis. 26. OTTI Symposium Thermische Solarenergie, Bad Staffelstein

Leibbrandt; Schabbach; Weber, 2014. Flachkollektoren aus Glas – erste Untersuchungsergebnisse. 24. OTTI Symposium Thermische Solarenergie, Bad Staffelstein

Rhein; Schabbach; Dölz; Leibbrandt, 2016. Strukturanalyse eines Nurglaskollektors unter Berücksichtigung statischer und dynamischer Lasten. 26. OTTI Symposium Thermische Solarenergie, Bad Staffelstein

Stephan, F. 2016. Experimentelle Untersuchung zur vollvolumetrischen Durchströmung eines Nurglaskollektors. Hochschule Nordhausen, Bachelor Thesis

Wesselak et al. 2013. Regenerative Energietechnik, 2. ed. Springer Vieweg, Berin, Heidelberg